Global impact of COVID-19 lockdown on surface concentration and health risk of atmospheric benzene

Chaohao Ling[a,1], Lulu Cui[d,1], Rui Li[b, c *]

[a] *School of History and Geography, Minnan Normal University, Zhangzhou, 363000, China*

[b] *Key Laboratory of Geographic Information Science of the Ministry of Education, School of Geographic Sciences, East China Normal University, Shanghai, 200241, PR China*

[c] *Institute of Eco-Chongming (IEC), 20 Cuiniao Road, Chenjia Town, Chongming District, Shanghai, 202162, China*

[d] *State Key Joint Laboratory of Environment Simulation and Pollution Control, School of Environment, Tsinghua University, Beijing, 100084, China*

[1]Chaohao Ling and Lulu Cui contributed to this work equally

*** Correspondence to:**

Prof. Li (rli@geo.ecnu.edu.cn)

Abstract

To curb the spread of COVID-19 pandemic, many countries around the world imposed an unprecedented lockdown producing reductions in pollutant emissions. Unfortunately, the lockdown-driven global ambient benzene changes still remained unknown. The ensemble machine-learning model coupled with the chemical transport models (CTMs) was applied to estimate global high-resolution ambient benzene levels. Afterwards, the XGBoost algorithm was employed to decouple the contributions of meteorology and emission reduction to ambient benzene. The change ratio (P_{dew}) of deweathered benzene concentration from pre-lockdown to lockdown period was in the order of India (-23.6%) > Europe (-21.9%) > United States (-16.2%) > China (-15.6%). The detrended change (P*) of deweathered benzene level (change ratio in 2020-change ratio in 2019) followed the order of India (P* = -16.2%) > Europe (P* = -13.9%) > China (P* = -13.3%) > United States (P* = -6.00%). Emission reductions derived from industrial activities and transportation were major drivers for the benzene decrease during lockdown period. The highest decreasing ratio of ambient benzene in India might be associated with local serious benzene pollution during the business-as-usual period and restricted transportation after lockdown. Substantial decreases of atmospheric benzene levels saved sufficient health benefits. The global average lifetime carcinogenic risks (LCR)

and hazard index (HI) decreased from 4.89×10^{-7} and 5.90×10^{-3} and 4.51×10^{-7} and 5.40×10^{-3}, respectively. China and India showed the higher health benefits due to benzene pollution mitigation compared with other countries, highlighting the importance of benzene emission reduction.

1. Introduction

Volatile organic compounds (VOCs) are an important class of organic pollutants in the urban air and have aroused great attention (Kamal et al., 2016; Koppmann, 2008; Mozaffar and Zhang, 2020). As one of the typical toxic VOC species, benzene poses a variety of negative impacts on human health including respiratory irritation, asthma, and allergies (Cui et al., 2019; Kim et al., 2013; Tang et al., 2007). Moreover, benzene has high chemical reactivity, and could participate in photochemical reactions in the atmosphere, thereby leading to the formation of secondary organic aerosols (SOA) and ozone (Dumanoglu et al., 2014; Hsu et al., 2018; Li et al., 2019). Given the high toxicity to human health and tremendous harm to air quality (Dumanoglu et al., 2014; Lu et al., 2020), it is highly imperative to decrease the ambient benzene concentration. It was well documented that ambient benzene mainly originated from anthropogenic emission (Mozaffar and Zhang, 2020; Pakkattil et al., 2021). Therefore, understanding the response of ambient benzene to anthropogenic emission was favorable to evaluate the effectiveness of abatement strategies and inform policy decisions.

Recently, the ongoing global outbreak COVID-19 has resulted in paroxysmal public health responses including travel restrictions, lockdown, curfews, and quarantines around the world. These drastic lockdown measures inevitably triggered sweeping disruptions of social and economic activities, and further affected the emissions and concentrations of some air pollutants (Bauwens et al., 2020; Berg et al., 2021; Doumbia et al., 2021; Zheng et al., 2021b). The unexpected public health emergency provided us an unprecedented chance to assess the response of air pollutants to emission reduction. Bauwens et al. (2020) has observed that the average NO_2 column in China during January-April 2020 decreased by about 40% relative to the same period in 2019 due to the dramatic decreases of NO_x emissions. Later on, Keller et al. (2021) has analyzed the impact of COVID-19 lockdown on global NO_2 concentrations and found that the surface NO_2 concentrations were 18% lower than business as usual from February 2020 onward. In addition, Hammer et al. (2021) estimated that population-weighted mean $PM_{2.5}$ concentrations in China, Europe, and North

America experienced changes of -11 to -15, -2 to 1, and -2 to 1 μg/m^3 during COVID-19 lockdown period, respectively. Compared with NO_2 and $PM_{2.5}$, ambient SO_2 levels in China (-4.6%) and India (-14%) did not experience marked variations after lockdown (Zhang et al., 2021; Zhao et al., 2020). It should be noted that the global O_3 concentration even increased up to 50% during this period (Keller et al., 2021). To date, most of the current studies focused on regional or global criteria pollutant (e.g., $PM_{2.5}$, NO_2, and O_3) concentration changes after the COVID-19 outbreak, while few studies assessed the impact of COVID-19 lockdown on ambient benzene levels.

Currently, only several studies assessed the impact of COVID-19 lockdown on atmospheric benzene level. Mor et al. (2021) observed that the atmospheric benzene level in Chandigarh, India decreased by 27% during COVID-19 period. Afterwards, Pakkattil et al. (2021) demonstrated that the ambient benzene levels in Delhi (-93%) and Mumbai (-72%) have suffered from drastic decreases after COVID-19 lockdown. In China, Pei et al. (2022) revealed the VOC concentration in Pearl River Delta (PRD) decreased by 19% and the decrease rate of ambient benzene reached ~40% after lockdown. In Europe, Cai et al. (2022) revealed that the ambient benzene level in Orléans even slightly increased after lockdown, which might be associated with the unfavorable meteorological conditions. Although the ground-level measurement could reflect the regional ambient benzene changes during COVID-19 lockdown period to some extents, few regions, especially in developing countries, have collected sufficient observations for ambient benzene exposure assessment (Geddes et al., 2016; Van Donkelaar et al., 2015). Moreover, the limited monitoring sites around the world cannot accurately reflect the global benzene pollution because of large spatial gaps and restricted spatial representativeness of these ground-based sites (Shi et al., 2018). The health effect assessment based on these scarce sites alone inevitably increased the probability of exposure misclassification (Ling and Li, 2021). Fortunately, chemical transport models (CTMs) gave us an unparalleled chance to capture the full-coverage ambient benzene level at the global scale. Although CTMs generally showed various biases owing to high uncertainties in initial conditions, input variables, and parameterizations (Ivatt and Evans, 2020), the machine-learning bias-correction method could significantly reduce bias in air quality models (Bocquet et al., 2015). Up to date, some studies have developed multiple machine-learning models to estimate the concentrations of $PM_{2.5}$ (Wei et al., 2021; Wei et al., 2020), NO_2 (Wei et al., 2023), and O_3 (Wei et al., 2022) around the world.

Unfortunately, no study employed the ensemble technique to analyze the change of global ambient benzene after COVID-19 outbreak. Besides, nearly all of the current studies only used original observation data to assess the impact of COVID-19 lockdown on ambient benzene level (Pakkattil et al., 2021). Actually, the concentrations of air pollutants were not only controlled by emission, but also modulated by complex meteorological conditions (Hammer et al., 2021). For instance, some pioneering studies have revealed that several severe haze episodes still occurred even with the strict restrictions put in place in China (Chang et al., 2020; Huang et al., 2021). Hence, it is necessary to remove the effects of meteorological parameters and then to further quantify the isolated contribution of emission reduction to global ambient benzene level and health risks during COVID-19 lockdown period.

In our study, the machine-learning model coupled with CTMs was applied to estimate the global ambient benzene concentrations from 23 January to 30 June in 2019 and 2020. At first, the CTMs output, emission inventory, meteorological parameters, and many other geographical covariates were integrated into the ensemble decision tree model to obtain global full-coverage benzene concentrations in the atmosphere. Then, we also examined the synergetic impacts from the anthropogenic emissions and meteorological factors during the pre-lockdown and lockdown periods. Finally, we estimated the emission-induced benzene concentrations before and after COVID-19 lockdown and quantified the benzene-related health benefits due to COVID-19 lockdown in major regions around the world. This study shows important implications for developing control strategies to alleviate global atmospheric benzene pollution.

2. Data and methods

2.1 Data preparation

2.1.1 Ground-level benzene observation

Our analysis was performed based on the recent development of unprecedented public access to ground-level air quality observations. In our study, we collected an air quality dataset of hourly surface benzene observations at 669 sites at the global scale during 23 January-30 June in 2019 and 2020 (Figure S1). The start date of COVID-19 lockdown in China was January 23th and the national lockdown lasted for about one month. However, the deblocking date in Wuhan was April 8th. The start and end dates of lockdown in India were March 25th and April 25th, respectively. The lockdown in the United States occurred firstly in California in March 19th, and then the lockdown lasted for 1-2 months. The lockdown dates in most European countries lasted from March to May. The detailed spatial distribution of these sites in India, Europe, and the United States are depicted in Figure S1. The surface benzene dataset in India was downloaded from the Central Pollution Control Board (CPCB) online database, which has been widely utilized in previous studies (Mahato et al., 2020; Mor et al., 2021; Sharma et al., 2020). The CPCB database provides data quality assurance (QA) or quality control (QC) programs by developing strict procedures for sampling, analysis, and calibration (Gurjar et al., 2016). The ground-level benzene observations in Europe and the United States were collected from air quality data portal of the European Environment Agency (EEA) and United States Environmental Protection Agency (EPA), respectively. Only days with more than 12 h of available data are included in the analysis. All of the hourly data was average to the daily scale.

2.1.2 Independent variables

The daily benzene concentrations at global scale were simulated using GEOS-Chem model (v12-01), which included the full gaseous HO_x-O_x-NO_x-CO-NMVOC chemistry and online aerosol calculations. The simulation used assimilated meteorological observations (GEOS MERRA-2) at 2° x 2.5° horizontal resolution with 72 vertical levels for the year 2019 and 2020. The anthropogenic emission inventory in 2019 was collected from Community Emissions Data System (CEDS). Then, the emission inventory in 2020 was calculated based on that in 2019 and updated adjustment factor proposed by Doumbia et al. (2021).

The meteorological parameters were obtained from the NASA Goddard Earth Observing System Composition Forecast (GEOS-CF) model (Keller et al., 2021b). GEOS-CF integrates the GEOS-Chem atmospheric chemistry model into the GEOS Earth System Model (Hu et al., 2018; Long et al., 2015) and provides global hourly analyses of meteorological variables at 0.25° spatial resolution (Keller et al., 2021b). Meteorological parameters including surface pressure (PS), relative humidity (RH), 2-m air temperature (T2M), total precipitation (TPREC), 10-m latitudinal wind component (U10M), 10-m longitudinal wind component (V10M), and boundary layer height (BLH) obtained from GEOS-CF were used to develop the model (Figure S2). In addition, cropland, forest, grassland, shrubland, and barren land also have been integrated into the final model (Liu et al., 2020).

All of the independent variables collected from multiple sources were regridded to 0.25° grids using spatial interpolation algorithms. During the process of model development, the most important procedure was to remove some redundant explanatory variables and then to determine the optimal variable group. The basic principle of the variable selection was to eliminate the less important predictors. These variables generally suggested that the R^2 value of the submodel did not experience a significant decrease or even suffered from a slight increase when these redundant ones were removed from the model. At last, a total of 64001 samples and 7 variables were utilized to predict the ambient benzene concentrations at the global scale.

2.2 Model development

2.2.1 The ensemble model development for atmospheric benzene estimates

In the pioneering studies, random forest (RF), extreme gradient boosting (XGBoost), and light gradient boosting machine (LightGBM) exhibited the better estimation accuracy (Li et al., 2021). RF model holds a great deal of decision trees, and each one experiences an independent sampling procedure and all of these trees show the same distributions (Breiman). RF model often displays excellent prediction performance owing to the injected randomness. The model accuracy is strongly dependent on the number of trees, splitting features, and the variable group. The detailed procedures are summarized as follows:

$$f(x)=\sum_{z=1}^{Z}c_z R(x\in Q_z)\ (1)$$

$$\overset{\Delta}{c_z}=average(y_i\mid x_i\in Q_z)\ (2)$$

$$BR_1(p,q)=\{X\mid X_j\le q\}\ \&\ BR_2(p,q)=\{X\mid X_j>q\}\ (3)$$

$$\min_{p,q}\left[\min\sum_{M_1(p,q)}(y-c_1)^2+\min\sum_{M_2(p,q)}(y-c_2)^2\right]\ (4)$$

$$\overset{\Delta}{c_1}=average(y_i|x_i\in Q_1(p,q))\&\overset{\Delta}{c_2}=average(y_i|x_i\in Q_2(p,q))\ (5)$$

where (x_i, y_i) is the sample for i = 1, 2, …, N in Q regions (Q_1, Q_2, …, Q_z); R denotes the weight of each branch; BR represents decision tree branch; c_m is the response to the model; $\overset{\Delta}{c_z}$ represents the optimal value, p is the feature variable; c_1 is the average of left branch; c_2 is the average of right branch; q represents the split point.

XGBoost model is an improved algorithm of gradient boosting decision tree (GBDT) model and loss functions have been extended to the second order function. The detailed XGBoost algorithm is shown as the following formula (Zhai and Chen, 2018):

$$Y^{(t)} = \sum_{i=1}^{n}[l(y_i, \hat{y}^{(t-1)}) + \partial_{y^{(t-1)}} l(y_i, \hat{y}^{(t-1)}) f_t(x_i) + \frac{1}{2}\partial^2_{y^{(t-1)}} l(y_i, \hat{y}^{(t-1)}) f_t^{2}(x_i)] + \varepsilon(f_t) \quad (6)$$

where $Y^{(t)}$ is the cost function at the t-th period; ∂ represents the derivative of the original function; $\partial^2_{y^{(t-1)}}$ is the second derivative of the original function; l is the differentiable convex loss function that reflects the minus of the predicted value ($\hat{y}$) of the i-th instance at the t-th period and the target value (y_i); $f_t(x)$ represents the increment; $\varepsilon(f_t)$ is the regularizer.

LightGBM model is an update version of XGBoost method, and significantly improve the running speed of modelling process. Moreover, this method could decrease the cache miss by a large margin and further improved the predictive accuracy. The detailed algorithms are as follows (Sun et al., 2020):

$$\hat{f} = \arg\min_{f} L(y, f(x)) \quad (7)$$

$$f_T(X) = \sum_{t=1}^{T} f_t(X) \quad (8)$$

$$\Gamma_t = \sum_{i=1}^{n}(g_i f_t(x_i) + \frac{1}{2} h_i f_t^{2}(x_i)) \quad (9)$$

where $\hat{f}$ is the least value of cost function; L(y, f(x)) is the cost function; $f_T(X)$ denotes the total regression trees; $f_t(X)$ represents each regression tree; g_i and h_i represent the first- and second-order gradient statistics of the cost function, respectively.

Although all of these models showed the better performance in predicting air pollutants, nearly all of these submodels still suffered from some weaknesses in the prediction accuracy. Hence, it was necessary to collocate these models using back-propagation neutral network (BPNN) to further simulate daily ambient benzene concentrations at the global scale. As depicted in Figure 1, three submodels including RF, XGBoost, and LightGBM were stacked through BPNN model to simulate the daily atmospheric benzene levels at the global scale. Firstly, a 5-fold cross-validation method was utilized to train each submodel to determine the optimal hyperparameter. Then, the BPNN method was employed to further train the estimated concentrations of three submodels against the observations (Figure 1). Lastly, the global ambient benzene concentrations were predicted on the basis of the ensemble model.

2.2.2 The meteorology-normalized benzene estimates

The ambient benzene concentration was influenced by both of meteorological parameters and emissions. To isolate the contribution of emission, the impacts of meteorological conditions should be removed. In our study, the XGBoost approach was utilized to eliminate the impacts of meteorological conditions. The simulated benzene concentration in each grid (0.25°) based on the method in section 2.2.1 was treated as the dependent variable. The daily benzene emission, meteorological factors, month of year (MOY), and day of year (DOY) in each grid were regarded as the explanatory variables. The raw dataset was randomly classified into a training dataset (90% of input dataset) for developing the XGBoost model and the remained samples were regarded as the test dataset. After the development of the XGBoost model, the weather normalized technique was employed to predict the ambient benzene concentration at a specific time point. The detailed deweathered algorithms was introduced by Grange and Carslaw (2019) firstly. The meteorology-normalized benzene level served as the concentrations contributed by emission alone. The differences of total and deweathered benzene concentrations were regarded as the concentration contributed by meteorology. In addition, the CV R^2 value of model using for the separation of meteorology and emission also should be higher than 0.50, otherwise the model could be considered to be unreliable.

2.3 Health effect assessment

In our study, the carcinogenic and non-carcinogenic risks of ambient benzene were assessed based on the standard methodology of United States Environmental Protection Agency (USEPA). The carcinogenic and non-carcinogenic risks induced by benzene exposure for were evaluated based on the lifetime carcinogenic risks (LCR) and hazard index (HI). The formulas for calculating benzene intake (BI), LCR, and HI are as follows (Table S1):

$$BI=(C\times ET\times EF\times ED)/(365\times 24\times AT) \quad (10)$$

$$HI=BI/RfC \quad (11)$$

$$LCR = BI \times IUR \tag{12}$$

where C (μg/m^3) denotes the concentration of the corresponding ambient benzene; ET is the exposure time; EF represents the annual exposure frequency (d a^{-1}); ED is the exposure duration (a); AT_{nca} and AT_{ca} denotes the average exposure time for carcinogenic and non-carcinogenic risks (a), respectively. BI means the benzene intake; RfC represents the reference dose (μg/m^3); IUR is the inhalation risk (1/μg/m^3). The non-carcinogenic risk of the ambient benzene is considered to be high when HI was above 1.0, whereas the health risk is not obvious when HI is below 1.0. The carcinogenic risk was regarded as definite risk when LCR was higher than 1×10^{-4}, while it was treated as the possible risk when this indicator was located between 1×10^{-6} and 1×10^{-4}. The risk was treated as negligible when the indicator was lower than 1×10^{-6} (Dumanoglu et al., 2014; Li et al., 2017).

3. **Results and discussion**

3.1 The model fitting and validation

The ensemble model was utilized to estimate the ambient benzene concentrations at the global scale during 23 January-30 June in 2019 and 2020. The cross-validation (CV) R^2 value of the ensemble model ($R^2 = 0.60$) was significantly higher than that of RF (0.52), XGBoost (0.53), and LightGBM (0.55) (Figure S3). Nevertheless, both of the root-mean-square error (RMSE) (1.18 μg/m^3) and the mean absolute error (MAE) (0.59 μg/m^3) of the ensemble model were significantly lower than those of RF (RMSE and MAE: 1.41 and 0.72 μg/m^3), XGBoost (RMSE and MAE: 1.37 and 0.70 μg/m^3), and LightGBM (RMSE and MAE: 1.34 and 0.69 μg/m^3). The higher R^2 value and the lower RMSE and MAE suggested the higher accuracy of the ensemble model in air quality simulation. In the pioneering studies, Wolpert (1992) confirmed that the joint use of multiple statistical models could decrease the probability of overfitting and strengthen the predictive accuracy and transferability of final models. Besides, our previous studies also demonstrated that the stacking of various decision tree models could significantly outperform individual model because each decision tree model could suffer from some weaknesses (Li et al., 2021). For instance, the dataset in the RF model appeared to be over-fitted when much noise existed in the training data of regression problems (Breiman, 2001). Besides, RF model might underestimated/overestimated the extremely values of ambient benzene (Xue et al., 2019), which could be neutralized by the XGBoost algorithm through the boosting method (Li et al., 2020). For XGBoost algorithm, excessive leaf nodes often showed low splitting gain, while the LightGBM model could make up this defect (Nemeth et al., 2019). Overall, the combination of these decision tree models could overcome these weaknesses of these individual models and enhance the robustness of the final model.

Although 10-fold CV has verified that the modelling performance of ensemble model was superior to the individual models, this method cannot examine the spatial transferability of this model. In our study, many regions except India, Europe, and the United States were lack of monitoring sites of ambient benzene. Fortunately, the CTMs output provided a strong proxy to predict the daily ambient benzene concentrations before and after COVID-19 outbreak. In order to examination the spatial transferability of the ensemble model, the cross validation was performed. In each round, two-thirds of the benzene dataset in India, Europe, and the United States were applied to train the model and the remained one was utilized to examine the model (e.g., India+Europe for training and the United States for testing). After three rounds, all of the simulated benzene concentrations were compared with the corresponding observed values. As shown in Figure S4, the out-of-bag R^2 value reached 0.58, which was slightly lower than the R^2 value (0.60) of training model. In addition, RMSE and MAE of the fitting equation for the out-of-bag data were 1.18 and 0.62, respectively. The result was in good agreement with those based on CV database, indicating the ensemble model showed satisfied spatial generalization.

The ensemble model can capture the spatiotemporal variation of ambient benzene during COVID-19 lockdown period, while the impact of COVID-19 lockdown cannot be quantified because the contribution of meteorological parameters cannot be removed based on this model alone. Therefore, it is proposed to employ the XGBoost algorithm to isolate the contribution of emission reduction to global atmospheric benzene. As depicted in Figure S5, the CV R^2 value and slope of fitting curve reached 0.65 and 0.62, respectively. The result suggested that meteorology-normalized model was robust because the CV R^2 value was much higher than 0.50.

3.2 The impact of COVID-19 lockdown on global atmospheric benzene level

The ensemble model was developed to expand the ground-observed benzene measurement to the global scale and capture the global spatial variability of ambient benzene. As shown in Figure S6, the global simulated (total) benzene concentration during Jan. 23-Jun. 30 in 2019 and 2020 ranged from 0.52 to 6.36 μg/m^3, with the average value of 0.92 ± 0.23 μg/m^3. At the regional scale, the benzene concentration displayed significantly spatial variability. The benzene concentration followed the order of India (1.44 ± 0.14 μg/m^3) > China (1.17 ± 0.13 μg/m^3) > Europe (1.02 ± 0.08 μg/m^3) > United States (0.96 ± 0.09 μg/m^3) during Jan. 23-Jun. 30 in 2019 and 2020. Besides, the global simulated mean benzene level suffered from slight decrease from 0.93 ± 0.06 in 2020 to 0.90 ± 0.06 in 2019. However, the inter-annual variation of ambient benzene exhibited remarkable spatial discrepancy at the global scale. As depicted in Figure S7, the change ratio of simulated (total) benzene level during the COVID-19 lockdown period (the difference of the benzene level before COVID-19 lockdown and that during COVID-19 lockdown period) in 2020 was in the order of India (-18.5%) > Europe (-16.7%) > China (-11.7%) > United States (-11.5%). Compared with 2020, the change ratio of benzene level during the same period in 2019 followed the order of India (-16.3%) > Europe (-6.62%) > United States (-6.46%) > China (-4.18%). It should be noted that the simulated ambient benzene concentration suffered from the higher decreasing ratio in 2020 compared with the same period in 2019 in nearly all of the major countries around the world, which might be associated with the local COVID-19 lockdown measures in 2020.

Due to the interference of meteorological conditions, we cannot quantify the direct impact of COVID-19 lockdown on ambient benzene based on the comparison of simulated (total) benzene levels. Thus, the meteorology-normalized method was employed to decouple the separated contributions of emission reduction and meteorology to ambient benzene. In our study, both of the change ratio and detrended change ratio were applied to evaluate the impact of COVID-19 lockdown on global ambient benzene level. The change ratio represents the variation of ambient benzene level during lockdown period in 2020 compared with pre-lockdown period in 2020. However, the detrended change ratio reflects the difference of the change ratio in 2020 and the change ratio during the same period in 2019, which could avoid the inter-annual system error and contingency of a single year. As summarized in Figure 2 and 3, the change ratio of deweathered benzene concentration from pre-lockdown to lockdown period in 2020 was in the order of India (-23.6%) > Europe (-21.9%) > United States (-16.2%) > China (-15.6%). Meanwhile, the change ratio of deweathered benzene concentration during the same time in 2019 followed the order of Europe (-10.2%) > United States (-8.04%) > India (-7.40%) > China (-2.31%). The large gap in the change ratio of deweathered benzene level between 2019 and 2020 confirmed that the drastic and consequential quarantines significantly decreased the ambient benzene concentrations in nearly all of the regions with lockdown measures. Among all of the major countries, India suffered from the most dramatic benzene decrease during 24 March 2020-24 April 2020 (-23.6%) compared with the same period in 2019 (-7.4%). During this period, the prohibition of industrial activities and mass transportation was proposed to curb the spread of COVID-19 pandemic, leading to the tremendous reduction of anthropogenic benzene emission (Pathakoti et al., 2021; Zhang et al., 2021). Sahu et al. (2022) revealed that the substantial increase of OH radical during COVID-19 period also facilitated the ambient benzene removal due to the photooxidation reaction. The decrease ratio of deweathered benzene level in India was close to that of $PM_{2.5}$ (-26%), while it is was markedly lower than that of NO_2 (-50%) (Zhang et al., 2021). Although both of Europe and the United States also performed stringent lockdown restrictions in some regions such as Italy, Spain, and California (Guevara et al., 2021a; Keller et al., 2021a), while the detrended change (P*: change ratio in 2020-change ratio in 2019) for deweathered benzene in Europe (P* = -13.9%) and the United States (P* = -6%) between 2020 and 2019 was still lower than that of India (P* = -16.2%) (Table 1). It was assumed that the absolute concentration of ambient benzene in Europe and the United States were much lower than that in India. It should be noted that the China displayed relatively gentle decreasing ratio (-15.6%) after COVID-19 outbreak, which was even lower than the ratio in the United States. As the first epidemic epicenter country, Chinese government imposed a rapid lockdown measure in Wuhan and other cities across China in an effort to prevent the spread of the COVID-19 pandemic (Wu et al., 2020). These restrictions interrupted a wide array of economic activities and reduced primary air pollutant emissions, and thus resulted in the remarkable decreases of deweathered NO_2 (-43.6%) and $PM_{2.5}$ (-22%) (Dai et al., 2021). The gentle decreasing ratio of ambient benzene compared with other pollutants might be linked with the source apportionment of atmospheric benzene. It was well known that industrial source (e.g., chemical industry and solvent use) was major emission sector of benzene (Li et al., 2019). Although the contribution from solvent use exhibited substantial decreases in some cities (Qi et al., 2021; Wang et al., 2021), the chemical industry was not entirely interrupted even during the COVID-19 lockdown period (Dai et al., 2021). Zheng et al. (2021a) also demonstrated that the reduction of non-methane volatile organic compounds (NMVOCs) emission from industry sector was much less than other pollutants.

Although the deweathered benzene concentrations in nearly all of the major countries experienced obvious decreases during COVID-19 lockdown period, the change ratios of deweathered benzene in different regions of these countries still showed large spatial variability. In China, most of the cities in East China such as Beijing (-30.6%), Shanghai (-6.25%), and Wuhan (-45.3%) experienced dramatic decreases of deweathered benzene levels (Figure S8), which was mainly contributed by the simultaneous emission reduction of industry and transportation sectors. Besides, enhanced atmospheric oxidation capacity could accelerate the benzene removal due to the unbalanced decreases of VOC and NO_x emissions (Jensen et al., 2021). However, the deweathered benzene concentrations in Northeast China and Yunnan province even exhibited slight increases after COVID-19 outbreak (Figure 4). Dai et al. (2021) also found that the deweathered $PM_{2.5}$ concentration in Kunming increased ~20% after COVID-19 outbreak. At first, the contribution of residential combustion source (62.1%) to atmospheric benzene in Yunnan province was higher than other sectors (Guevara et al., 2021b; Kuenen et al., 2021). Moreover, the increase of domestic emission due to home quarantine order further increased the ambient benzene concentration (10%) in this province, which has been demonstrated by the updated emission inventory in 2020 (Doumbia et al., 2021). The slight increases of deweathered benzene levels in Northeast China after COVID-19 outbreak could be linked with the earlier work resumption(https://baijiahao.baidu.com/s?id=1658138056285012986&wfr=spider&for=pc). Based on the simulation result, the deweathered ambient benzene level in Northeast China rebounded sharply after the third week, and then returned back to normal in the late February. In India, the decreasing ratios of deweathered benzene in Delhi, Mumbai, Kolkata, Bengaluru, Hyderabad, Chennai, Ahmedabad, and Lucknow reached 21.6%, 20.9%, 73.7%, 26.9%, 38.0%, 33.7%, 25.1%, and 33.3% during COVID-19 lockdown period (Figure S9), respectively. Among all of the major cities in India, the ambient benzene level in Kolkata suffered from the most drastic decrease. It was assumed that Kolkata is designated as dusty city and filled with vehicle emission. Fortunately, the city experienced complete stop of vehicles movement, burning of biomass and dust particles from the construction works, which were important sources for ambient benzene (Bera et al., 2021; Kumar and and Singh, 2003). In Europe, the deweathered benzene levels in nearly all of the cities displayed marked decreases because most European countries have imposed lockdowns to combat the spread of the COVID-19 pandemic (Guevara et al., 2021a). For example, the private car use and heavy good vehicles (HGVs) on the road in London reduced by 80% and 30-40%, respectively (Shi et al., 2021). The drastic decrease of transportation emission triggered the P* value in London between 2020 and 2019 reaching -43.6%. In the United States, the decreasing ratios of deweathered benzene levels in the cities of Eastern United States and California were generally higher than those in Central United States, which was in good agreement with the spatial variability of $PM_{2.5}$ decrease (Hammer et al., 2021). It was closely associated with the length of lockdown period (https://en.wikipedia.org/wiki/COVID-19_lockdowns).

In addition, ambient benzene levels were also strongly affected by meteorological conditions that alter photochemical production, advection, and depositional loss. Hence, we examined how meteorological parameters influenced the temporal variability of ambient benzene during COVID-19 lockdown period. In 2020, most of the major countries including China (3.9%), Europe (5.2%), and the United States (4.7%) suffered from slight unfavorable meteorological conditions, which was in good agreement with the impact of meteorological conditions on ambient NO_2 concentrations (Shi et al., 2021). Among all the meteorological parameters, air temperature was the most important factor for ambient benzene in nearly all of the regions around the world during the study period. Compared with 2019, the air temperatures in China, India, Europe, and the United States increased by 0.4, 0.9, 0.4, and 0.2℃ during the same period in 2020, respectively. Jia and Xu (2014) demonstrated that the increased air temperature generally suppressed the benzene photooxidation and secondary organic aerosol (SOA) formation. Thus, the increased air temperature was not beneficial to the further reduction of ambient benzene. Except air temperature, some other factors such as RH, rainfall amount, and wind speed might affect the ambient benzene level. For instance, the increased RH could be favorable to the benzene oxidation and the higher rainfall amount promoted the benzene removal. However, in the machine learning model, the importance values of these variables were much lower than that of air temperature. Overall, the result suggested that the unfavorable meteorological conditions (air temperature) weakened the health benefits of ambient benzene due to drastic lockdown measures around the world.

3.3 The effect of COVID-19 lockdown on global health risks

The global average LCR during 23 January-30 June in 2019 and 2020 were 4.89×10^{-7} and 4.51×10^{-7} after removing the contributions of meteorological conditions, respectively (Figure S10). Although the COVID-19 lockdown decreased the LCR value slightly, both of the LCR values during two periods were lower than the threshold level of 10^{-6}, suggesting that dwellings in most regions could avoid carcinogenic risk through inhalation exposure to benzene (Li et al., 2017). However, the LCR values showed significant spatial difference in different regions. For instance, North China often suffered from the relatively higher benzene pollution, and the LCR value in this region decreased from 1.03×10^{-6} (possible risk) during the study period in 2019 (the same period to 2020) to 7.37×10^{-7} during COVID-19 lockdown period. The result verified that the stringent emission control measures significantly decreased the health risk due to benzene exposure. The LCR value across India only decreased from 6.55×10^{-7} to 6.42×10^{-7} during the study period, whereas the northern part of India such as Bihar decreased from 1.14×10^{-6} to 1.09×10^{-6} due to the impact of COVID-19 lockdown (Figure 5). As the most populous province of India, Bihar possessed more than 124 million people (http://kolkata.china-consulate.org/chn/lqgk/t1331638.htm). The result suggested that the COVID-19 lockdown certainly obtained remarkable short-term health benefits through decreasing the ambient benzene exposure. The LCR values in Europe and the United States decreased from 4.99×10^{-7} and 4.77×10^{-7} to 4.57×10^{-7} and 4.63×10^{-7}, respectively. Compared with China and India, Europe and the United States suffered from relatively low carcinogenic risk of benzene exposure even before COVID-19 lockdown. Although the COVID-19 lockdown further decreased the LCR values in these regions, the overall carcinogenic risk was negligible.

Additionally, the non-carcinogenic risk around the world during the period was also assessed based on HI. The average HI of ambient benzene exposure in China, India, Europe, and the United States reduced from 8.92×10^{-3}, 7.45×10^{-3}, 6.32×10^{-3}, and 5.76×10^{-3} in 2019 to 8.53×10^{-3}, 7.13×10^{-3}, 5.81×10^{-3}, and 5.59×10^{-3} during COVID-19 lockdown period in 2020 (Figure 6), respectively. Although HI value in some regions including Bihar (1.52×10^{-2} to 1.41×10^{-2}) and Uttar Pradesh (1.04×10^{-2} to 1.03×10^{-2}) in India and Beijing-Tianjin-Hebei (BTH) (1.25×10^{-2} to 1.14×10^{-2}) in China still experienced decreases during COVID-19 lockdown period, the HI values in these regions were still significantly lower than the risk threshold (HI = 1). Therefore, the impact of COVID-19 lockdown on non-carcinogenic risk of benzene exposure was insignificant.

4. Conclusions and limitations

The drastic lockdown measures largely reduced the air pollutant emissions. The meteorology-normalized ambient benzene concentrations in China (-15.6%), India (-23.6%), Europe (-21.9%), and the United States (-16.2%) experienced dramatic decreases after COVID-19 outbreak. Furthermore, the decreasing ratios in these major regions during COVID-19 lockdown period were much higher than the same period in 2019, indicating the aggressive emission control measures efficiently decreased ambient benzene concentrations. Emission reductions from industrial activities and transportation were major drivers for the decreasing of ambient benzene level during lockdown period, while the relatively stable solvent use emission could restrict the further decrease of benzene pollution. Besides, the slight increase of domestic emission during this period might be an important reason for the benzene increase in some regions (e.g., Yunnan province). There is also an urgent need to control the household combustion and solvent use emissions apart from the emissions from industry and transportation sectors.

Besides, substantial decreases of atmospheric benzene levels could save sufficient health benefits. Dramatic decreases of benzene emissions in Europe and the United States cannot save effective health benefits because the ambient benzene levels in both of these regions during business-as-usual scenario were significantly lower than the risk threshold. However, the benzene decreases in North China Plain (NCP), China and Bihar, India could save abundant health benefits because these regions often suffered from severe atmospheric benzene pollution during business-as-usual scenario. Thus, more targeted abatement measures are needed to reduce the benzene emission in these areas. For instance, the stricter industrial and vehicle emission standards for VOC control should be implemented in China and India. Moreover, some measures including limiting the amount of coal-fired power plants, adding environmentally friendly cars and clean fuels for vehicles and vessels, and strengthening the labeling system for vehicles in use should be strengthened.

It should be noted that our study still suffered from some limitations. First of all, the monitoring sites were not evenly distributed around the world, and thus the simulation result might show the higher uncertainty in the regions lack of monitoring sites. Besides, the GEOS-Chem model still suffered from some uncertainties due to imperfect chemical mechanism and inaccurate emission inventory. In the future work, the model should be further improved.

Acknowledgements

This work was supported by the National Natural Science Foundation of China (42107113).

Data availability

The CEDS emission inventory are available at the website of https://zenodo.org/record/3754964#.YwrJL8jfmfU. The global meteorological parameters (reanalysis dataset) are obtained from the website of http://geoschemdata.wustl.edu/ExtData/.

Author contributions

LCH and LR wrote the manuscript. LR and CLL contributed to the conceptualization of the study. LCH and LR conducted the research, and visualized the results. CLL revised the manuscript.

Competing interests

The contact author has declared that neither they nor their co-authors have any competing interests.

References

Bauwens, M., Compernolle, S., Stavrakou, T., Müller, J. F., van Gent, J., Eskes, H., Levelt, P. F., van der A, R., Veefkind, J. P., Vlietinck, J., Yu, H., and Zehner, C.: Impact of coronavirus outbreak on NO_2 pollution assessed using TROPOMI and OMI observations. Geophy. Res. Lett., 47, e2020GL087978, 2020.

Bera, B., Bhattacharjee, S., Shit, P. K., Sengupta, N., and Saha, S.: Significant impacts of COVID-19 lockdown on urban air pollution in Kolkata (India) and amelioration of environmental health. Environ. Dev. Sustain., 23, 6913-6940, 2021.

Berg, K., Romer Present, P., and Richardson, K.: Long-term air pollution and other risk factors associated with COVID-19 at the census tract level in Colorado. Environ. Pollut., 287, 117584, 2021.

Bocquet, M., Elbern, H., Eskes, H., Hirtl, M., Žabkar, R., Carmichael, G., Flemming, J., Inness, A., Pagowski, M., and Pérez Camaño, J.: Data assimilation in atmospheric chemistry models: current status and future prospects for coupled chemistry meteorology models. Atmos. Chem. Phys., 15, 5325-5358, 2015.

Breiman, L.: Random forests. Machine learning 45, 5-32, 2001.

Cai, M., Yang, Y. G., Gibilisco, R. G., Grosselin, B., McGillen, M. R., Xue, C. Y., Mellouki, A., and Daële, V.: Ambient BTEX Concentrations during the COVID-19 Lockdown in a Peri-Urban Environment (Orléans, France). Atmosphere, 13, 10, 2022.

Chang, Y., Huang, R. J., Ge, X., Huang, X., Hu, J., Duan, Y., Zou, Z., Liu, X., and Lehmann, M. F.: Puzzling haze events in China during the coronavirus (COVID-19) shutdown. Geophy. Res. Lett., 47, e2020GL088533, 2020.

Cui, L., Li, R., Zhang, Y., Meng, Y., Zhao, Y., and Fu, H.: A geographically and temporally weighted regression model for assessing intra-urban variability of volatile organic compounds (VOCs) in Yangpu district, Shanghai. Atmos. Environ., 213, 746-756, 2019.

Dai, Q., Hou, L., Liu, B., Zhang, Y., Song, C., Shi, Z., Hopke, P.K., and Feng, Y.: Spring Festival and COVID-19 lockdown: disentangling PM sources in major Chinese cities. Geophy. Res. Lett., e2021GL093403, 2021.

Doumbia, T., Granier, C., Elguindi, N., Bouarar, I., Darras, S., Brasseur, G., Gaubert, B., Liu, Y., Shi, X., and Stavrakou, T.: Changes in global air pollutant emissions during the COVID-19 pandemic: a dataset for atmospheric modeling. Earth Syst. Sci. Data, 13, 4191-4206, 2021.

Dumanoglu, Y., Kara, M., Altiok, H., Odabasi, M., Elbir, T., and Bayram, A.: Spatial and seasonal variation and source apportionment of volatile organic compounds (VOCs) in a heavily industrialized region. Atmos. Environ., 98, 168-178, 2014.

Geddes, J. A., Martin, R. V., Boys, B. L., and van Donkelaar, A.: Long-term trends worldwide in ambient NO_2 concentrations inferred from satellite observations. Environ. Health Persp., 124, 281-289, 2016.

Grange, S. K. and Carslaw, D. C.: Using meteorological normalisation to detect interventions in air quality time series. Sci. Total Environ., 653, 578-588, 2019.

Guevara, M., Jorba, O., Soret, A., Petetin, H., Bowdalo, D., Serradell, K., Tena, C., Denier van der Gon, H., Kuenen, J., and Peuch, V. H.: Time-resolved emission reductions for atmospheric chemistry modelling in Europe during the COVID-19 lockdowns. Atmos. Chem. Phys., 21, 773-797, 2021a.

Guevara, M., Jorba, O., Tena, C., Denier van der Gon, H., Kuenen, J., Elguindi, N., Darras, S., Granier, C., and Pérez García-Pando, C.: Copernicus Atmosphere Monitoring Service TEMPOral profiles (CAMS-TEMPO): global and European emission temporal profile maps for atmospheric chemistry modelling. Earth Syst. Sci. Data, 13, 367-404, 2021b.

Gurjar, B. R., Ravindra, K., and Nagpure, A. S.: Air pollution trends over Indian megacities and their local-to-global implications. Atmos. Environ., 142, 475-495, 2016.

Hammer, M. S., van Donkelaar, A., Martin, R. V., McDuffie, E. E., Lyapustin, A., Sayer, A. M., Hsu, N. C., Levy, R. C., Garay, M. J., and Kalashnikova, O. V.: Effects of COVID-19 lockdowns on fine particulate matter concentrations. Sci. Adv., 7, eabg7670, 2021.

Hsu, C. Y., Chiang, H. C., Shie, R. H., Ku, C. H., Lin, T. Y., Chen, M. J., Chen, N. T., and Chen, Y. C.: Ambient VOCs in residential areas near a large-scale petrochemical complex: Spatiotemporal variation, source apportionment and health risk. Environ. Pollut., 240, 95-104, 2018.

Hu, L., Keller, C. A., Long, M. S., Sherwen, T., Auer, B., Da Silva, A., Nielsen, J. E., Pawson, S., Thompson, M. A., and Trayanov, A. L.: Global simulation of tropospheric chemistry at 12.5 km resolution: performance and evaluation of the GEOS-Chem chemical module (v10-1) within the NASA GEOS Earth system model (GEOS-5 ESM). Geosci. Model Dev., 11, 4603-4620, 2018.

Huang, X., Ding, A., Gao, J., Zheng, B., Zhou, D., Qi, X., Tang, R., Wang, J., Ren, C., and Nie, W.: Enhanced secondary pollution offset reduction of primary emissions during COVID-19 lockdown in China. Natl. Sci. Rev., 8, nwaa137, 2021.

Ivatt, P. D. and Evans, M. J.: Improving the prediction of an atmospheric chemistry transport model using gradient-boosted regression trees. Atmos. Chem. Phys., 20, 8063-8082, 2020.

Jensen, A., Liu, Z. Q., Tan, W., Dix, B., Chen, T. S., Koss, A., Zhu, L., Li, L., Gouw, J. D.: Measurements of volatile organic compounds during the COVID-19 lockdown in Changzhou, China. Geophys. Res. Lett., 48, e2021GL095560, 2021.

Jia, L., and Xu, Y. F.: Effects of relative humidity on ozone and secondaryorganic aerosol formation from the photooxidationof benzene and ethylbenzene. Aerosol Sci. Tech., 48, 1-12, 2014.

Kamal, M. S., Razzak, S. A., and Hossain, M. M.: Catalytic oxidation of volatile organic compounds (VOCs)–A review. Atmos. Environ., 140, 117-134, 2016.

Keller, C. A., Evans, M. J., Knowland, K. E., Hasenkopf, C. A., Modekurty, S., Lucchesi, R. A., Oda, T., Franca, B. B., Mandarino, F. C., and Díaz Suárez, M. V.: Global impact of COVID-19 restrictions on the surface concentrations of nitrogen dioxide and ozone. Atmos. Chem. Phys., 21, 3555-3592, 2021a.

Keller, C. A., Knowland, K. E., Duncan, B. N., Liu, J., Anderson, D. C., Das, S., Lucchesi, R. A., Lundgren, E. W., Nicely, J. M., and Nielsen, E.: Description of the NASA GEOS Composition Forecast Modeling System GEOS-CF v1. 0. J. Adv. Model Earth Sy., 13, e2020MS002413, 2021b.

Kim, K. H., Jahan, S. A., and Kabir, E.: A review on human health perspective of air pollution with respect to allergies and asthma. Environ. Int., 59, 41-52, 2013.

Koppmann, R.: Volatile organic compounds in the atmosphere. John Wiley & Sons, 2008.

Kuenen, J., Dellaert, S., Visschedijk, A., Jalkanen, J. P., Super, I., and Denier van der Gon, H.: CAMS-REG-v4: a state-of-the-art high-resolution European emission inventory for air quality modelling. Earth Syst. Sci. Data, 1-37, 2021.

Kumar, B., and Singh, R. B.: Urban development and anthropogenic climate change: experience in Indian metropolitan cities. Ltd, New Delhi, India: Manak Publication Pvt, 2003.

Li, B., Ho, S. S. H., Xue, Y., Huang, Y., Wang, L., Cheng, Y., Dai, W., Zhong, H., Cao, J., and Lee, S.: Characterizations of volatile organic compounds (VOCs) from vehicular emissions at roadside environment: The first comprehensive study in Northwestern China. Atmos. Environ., 161, 1-12, 2017.

Li, M., Zhang, Q., Zheng, B., Tong, D., Lei, Y., Liu, F., Hong, C., Kang, S., Yan, L., and Zhang, Y.: Persistent growth of anthropogenic non-methane volatile organic compound (NMVOC) emissions in China during 1990-2017: drivers, speciation and ozone formation potential. Atmos. Chem. Phys., 19, 8897-8913, 2019.

Li, R., Cui, L., Fu, H., Zhao, Y., Zhou, W., and Chen, J.: Satellite-based estimates of wet ammonium (NH_4-N) deposition fluxes across China during 2011-2016 using a space-time ensemble model. Environ. Sci. Technol., 54, 13419-13428, 2020.

Li, R., Cui, L., Zhao, Y., Zhou, W., and Fu, H.: Long-term trends of ambient nitrate (NO_3^-) concentrations across China based on ensemble machine-learning models. Earth Syst. Sci. Data, 13, 2147-2163, 2021.

Ling, C., and Li, Y.: Substantial changes of gaseous pollutants and health effects during the COVID-19 lockdown period across China. GeoHealth, e2021GH000408, 2021.

Liu, H., Gong, P., Wang, J., Clinton, N., Bai, Y., and Liang, S.: Annual dynamics of global land cover and its long-term changes from 1982 to 2015. Earth Syst. Sci. Data, 12, 1217-1243, 2020.

Long, M., Yantosca, R., Nielsen, J., Keller, C., Da Silva, A., Sulprizio, M., Pawson, S., and Jacob, D.: Development of a grid-independent GEOS-Chem chemical transport model (v9-02) as an atmospheric chemistry module for Earth system models. Geosci. Model Dev., 8, 595-602, 2015.

Lu, F., Li, S., Shen, B., Zhang, J., Liu, L., Shen, X., and Zhao, R.: The emission characteristic of VOCs and the toxicity of BTEX from different mosquito-repellent incenses. J. Hazard. Mater., 384, 121428, 2020.

Mahato, S., Pal, S., and Ghosh, K. G.: Effect of lockdown amid COVID-19 pandemic on air quality of the megacity Delhi, India. Sci. Total Environ., 730, 139086, 2020.

Mor, S., Kumar, S., Singh, T., Dogra, S., Pandey, V., and Ravindra, K.: Impact of COVID-19 lockdown on air quality in Chandigarh, India: understanding the emission sources during controlled anthropogenic activities. Chemosphere, 263, 127978, 2021.

Mozaffar, A., and Zhang, Y. L.: Atmospheric volatile organic compounds (VOCs) in China: A review. Curr. Pollut. Rep., 1-14, 2020.

Nemeth, M., Borkin, D., and Michalconok, G.: The comparison of machine-learning methods XGBoost and LightGBM to predict energy development, Proceedings of the Computational Methods in Systems and Software. Springer, pp. 208-215, 2019.

Pakkattil, A., Muhsin, M., and Varma, M. R.: COVID-19 lockdown: Effects on selected volatile organic compound (VOC) emissions over the major Indian metro cities. Urban Clim., 37, 100838, 2021.

Pathakoti, M., Muppalla, A., Hazra, S., D Venkata, M., A Lakshmi, K., K Sagar, V., Shekhar, R., Jella, S., MV Rama, S.S., and Vijayasundaram, U.: Measurement report: An assessment of the impact of a nationwide lockdown on air pollution-a remote sensing perspective over India. Atmos. Chem. Phys., 21, 9047-9064, 2021.

Pei, C. L., Yang, W. Q., Zhang, Y. L., Song, W., Xiao, S. X., Wang, J., Zhang, J. P., Zhang, T., Chen, D. H., Wang, Y. J., Chen, Y. N., and Wang, X. M.: Decrease in ambient volatile organic compounds during the COVID-19 lockdown period in the Pearl River Delta region, South China. Sci. Total Environ., 823, 153720, 2022.

Qi, J., Mo, Z., Yuan, B., Huang, S., Huangfu, Y., Wang, Z., Li, X., Yang, S., Wang, W., and Zhao, Y.: An observation approach in evaluation of ozone production to precursor changes during the COVID-19 lockdown. Atmos. Environ., 262, 118618, 2021.

Sahu, L. K., Tripathi, N., Gupta, M., Singh, V., Yadav, R., and Patel, K.: Impact of COVID-19 pandemic lockdown in ambient concentrations of aromatic volatile organic compounds in a metropolitan city of Western India. J. Geophy. Res. Atmos., 127, e2022JD036628, 2022.

Sharma, S., Zhang, M., Anshika, Gao, J., Zhang, H., and Kota, S. H.: Effect of restricted emissions during COVID-19 on air quality in India. Sci. Total Environ., 728, 138878, 2020.

Shi, X., Zhao, C., Jiang, J.H., Wang, C., Yang, X., and Yung, Y. L.: Spatial representativeness of $PM_{2.5}$ concentrations obtained using observations from network stations. J. Geophy. Res. Atmos., 123, 3145-3158, 2018.

Shi, Z., Song, C., Liu, B., Lu, G., Xu, J., Van Vu, T., Elliott, R. J., Li, W., Bloss, W. J., and Harrison, R. M.: Abrupt but smaller than expected changes in surface air quality attributable to COVID-19 lockdowns. Sci. Adv., 7, eabd6696, 2021.

Sun, X., Liu, M., and Sima, Z.: A novel cryptocurrency price trend forecasting model based on LightGBM. Financ. Res. Lett., 32, 101084, 2020.

Tang, J., Chan, L., Chan, C., Li, Y. S., Chang, C., Liu, S., Wu, D., and Li, Y.: Characteristics and diurnal variations of NMHCs at urban, suburban, and rural sites in the Pearl River Delta and a remote site in South China. Atmos. Environ., 41, 8620-8632, 2007.

Van Donkelaar, A., Martin, R. V., Brauer, M., and Boys, B. L.: Use of satellite observations for long-term exposure assessment of global concentrations of fine particulate matter. Environ. Health Persp., 123, 135-143, 2015.

Wang, M., Lu, S., Shao, M., Zeng, L., Zheng, J., Xie, F., Lin, H., Hu, K., and Lu, X.: Impact of COVID-19 lockdown on ambient levels and sources of volatile organic compounds (VOCs) in Nanjing, China. Sci. Total Environ., 757, 143823, 2021.

Wei, J., Li, Z., Lyapustin, A., Sun, L., Peng, Y., Xue, W., Su, T., and Cribb, M.: Reconstructing 1-km-resolution high-quality $PM_{2.5}$ data records from 2000 to 2018 in China: spatiotemporal variations and policy implications. Remote Sens Environ., 252, 112136, 2021.

Wei, J.*, Li, Z., Pinker, R., Wang, J., Sun, L., Xue, W., Li, R., and Cribb, M.: Himawari-8-derived diurnal variations of ground-level $PM_{2.5}$ pollution across China using the fast space-time Light Gradient Boosting Machine (LightGBM). Atmos. Chem. Phys., 21, 7863-7880, 2021. https://doi.org/10.5194/acp-21-7863-2021.

Wei, J., Li, Z., Li, K., Dickerson, R., Pinker, R., Wang, J., Liu, X., Sun, L., Xue, W., and Cribb, M.: Full-coverage mapping and spatiotemporal variations of ground-level ozone (O_3) pollution from 2013 to 2020 across China. Remote Sens Environ., 270, 112775, 2022.

Wei, J.*, Li, Z., Wang, J., Li, C., Gupta, P., and Cribb, M.: Ground-level gaseous pollutants (NO_2, SO_2, and CO) in China: daily seamless mapping and spatiotemporal variations. Atmos. Chem. Phys., 23, 1511-1532, 2023.

Wolpert, D. H.: Stacked generalization. Neural networks 5, 241-259, 1992.

Wu, J., Gamber, M., and Sun, W.: Does wuhan need to be in lockdown during the Chinese lunar new year? Multidisciplinary Digital Publishing Institute, 2020.

Xue, T., Zheng, Y., Tong, D., Zheng, B., Li, X., Zhu, T., and Zhang, Q.: Spatiotemporal continuous estimates of $PM_{2.5}$ concentrations in China, 2000-2016: A machine learning method with inputs from satellites, chemical transport model, and ground observations. Environ. Int., 123, 345-357, 2019.

Zhai, B., and Chen, J.: Development of a stacked ensemble model for forecasting and analyzing daily average $PM_{2.5}$ concentrations in Beijing, China. Sci. Total Environ., 635, 644-658, 2018.

Zhang, M., Katiyar, A., Zhu, S., Shen, J., Xia, M., Ma, J., Kota, S.H., Wang, P., and Zhang, H.: Impact of reduced anthropogenic emissions during COVID-19 on air quality in India. Atmos. Chem. Phys., 21, 4025-4037, 2021.

Zheng, B., Zhang, Q., Geng, G., Chen, C., Shi, Q., Cui, M., Lei, Y., and He, K.: Changes in China's anthropogenic emissions and air quality during the COVID-19 pandemic in 2020. Earth Syst. Sci. Data 13, 2895-2907, 2021a.

Zheng, P., Chen, Z., Liu, Y., Song, H., Wu, C. H., Li, B., Kraemer, M. U. G., Tian, H., Yan, X., Zheng, Y., Stenseth, N. C., and Jia, G.: Association between coronavirus disease 2019 (COVID-19) and long-term exposure to air pollution: Evidence from the first epidemic wave in China. Environ. Pollut., 276, 116682, 2021b.

Figure 1 The workflow of global atmospheric benzene modelling. CTM output represents the simulated benzene concentration based on GEOS-Chem model. Meteo denotes the meteorological parameters derived from GEOS-CF reanalysis. Emission represents the daily emission of benzene. MOY and DOY are the month of year and day of year, respectively. Simulated benzene represents the predicted benzene concentrations based on the ensemble model. Deweathered benzene denotes the benzene concentration after removing meteorological effects.

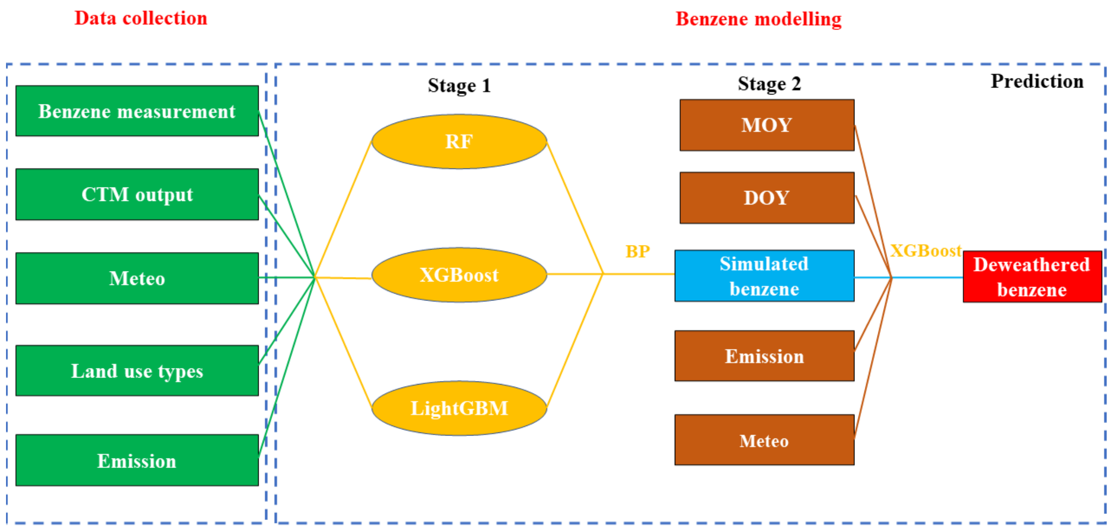

Figure 2 The global average deweathered benzene concentrations in 2019 (Jan. 23-Jun. 30) (a) and 2020 (Jan. 23-Jun. 30) (b). (c) represents the difference of deweathered benzene concentrations in 2020 and 2019 (Unit: μg/m^3).

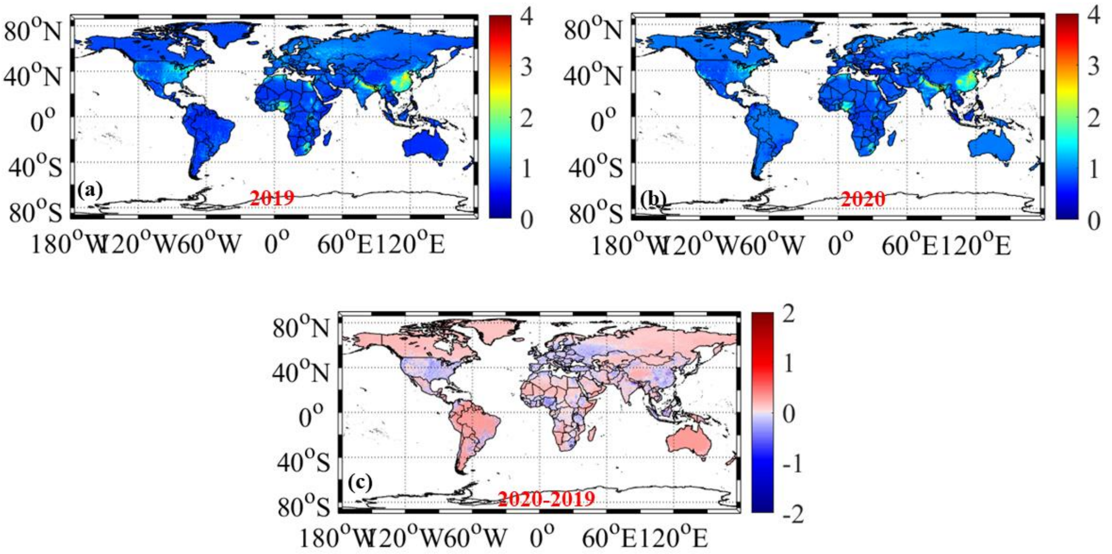

Figure 3 The weekly variations of atmospheric benzene concentrations (μg/m^3) in some major regions around the world during Jan. 23-Jun. 30. The red line and background denote mean values and standard deviation of deweathered weekly benzene concentrations in 2020. The cyan line and background denote mean values and standard deviation of deweathered weekly benzene levels in 2019. The dashed vertical red line suggests COVID-19 restriction dates, and the black line indicates the beginning of easing measures.

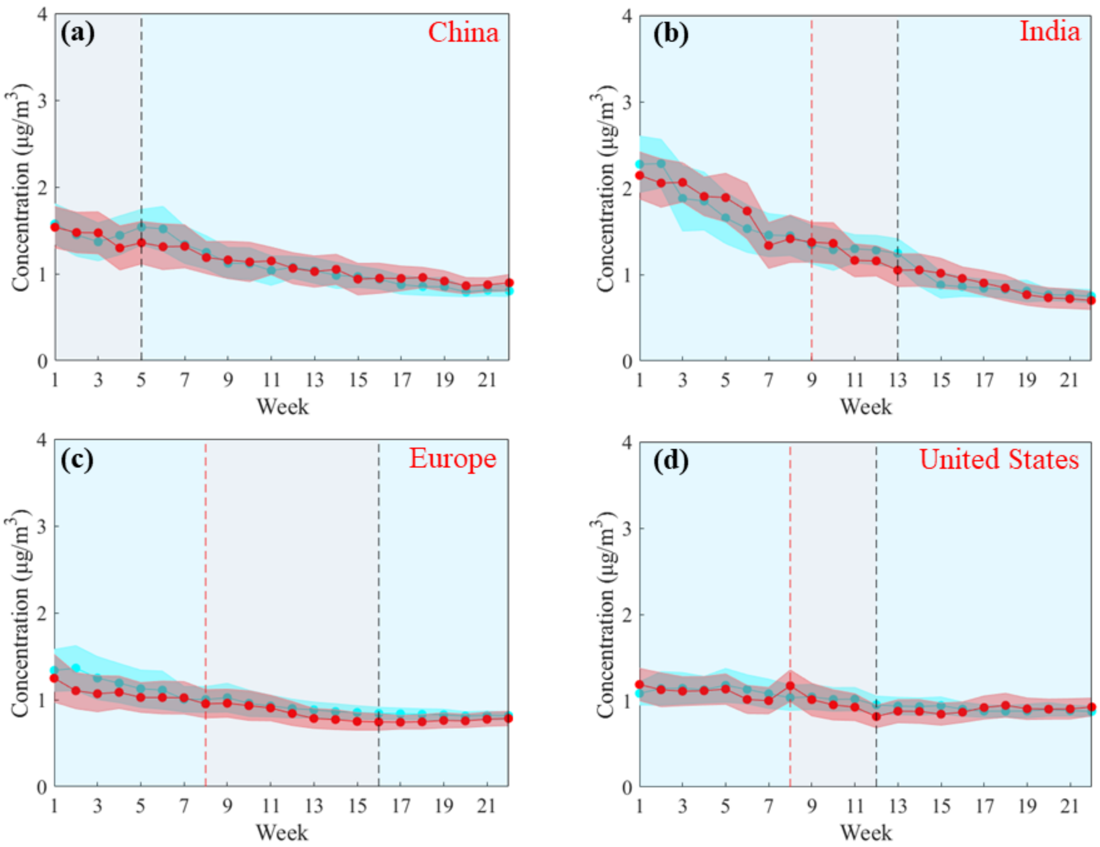

Figure 4 The concentration difference for deweathered benzene between COVID-19 period in 2020 and the same period in 2019 in East Asia, South Asia, Europe, and North America (Difference = deweathered benzene concentration in 2020-deweathered benzene concentration in 2019) (Unit: μg/m^3).

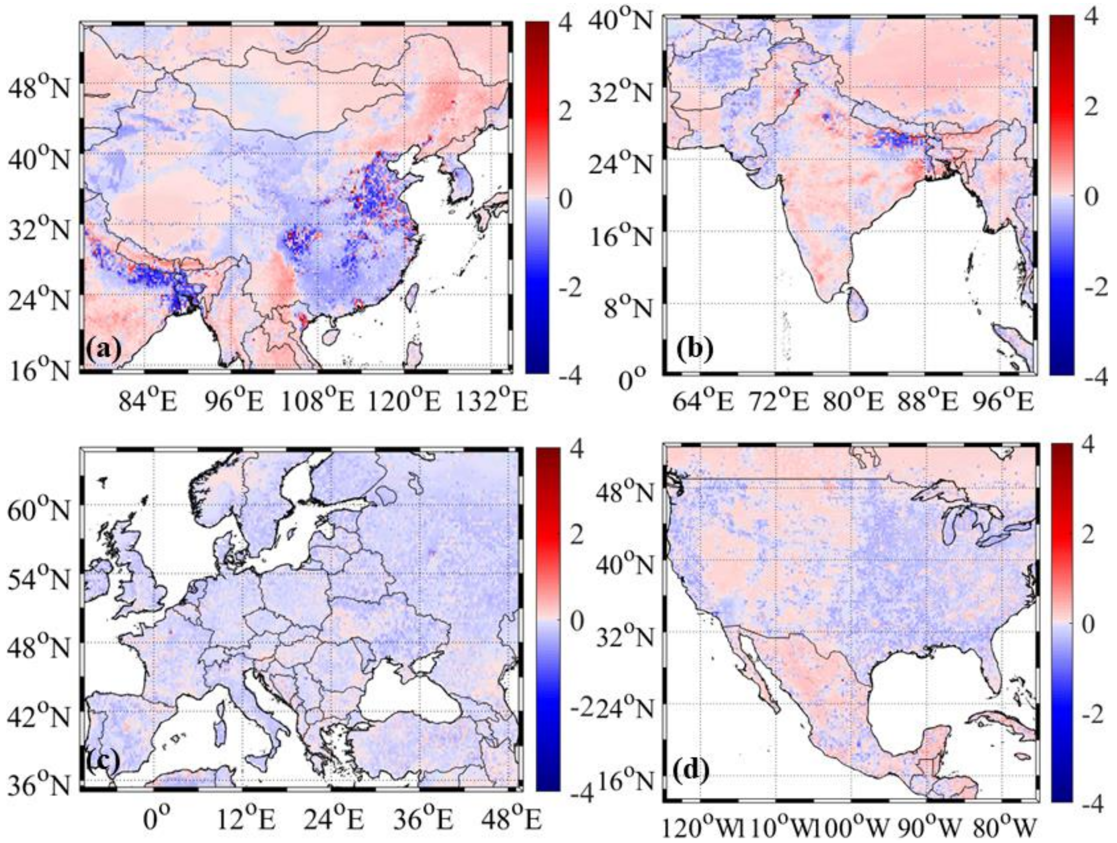

Figure 5 The carcinogenic risk differences (Unit: 10^{-7}) for atmospheric benzene between COVID-19 period in 2020 and the same period in 2019 in East Asia, South Asia, Europe, and North America (Difference = benzene concentration in 2020-benzene concentration in 2019).

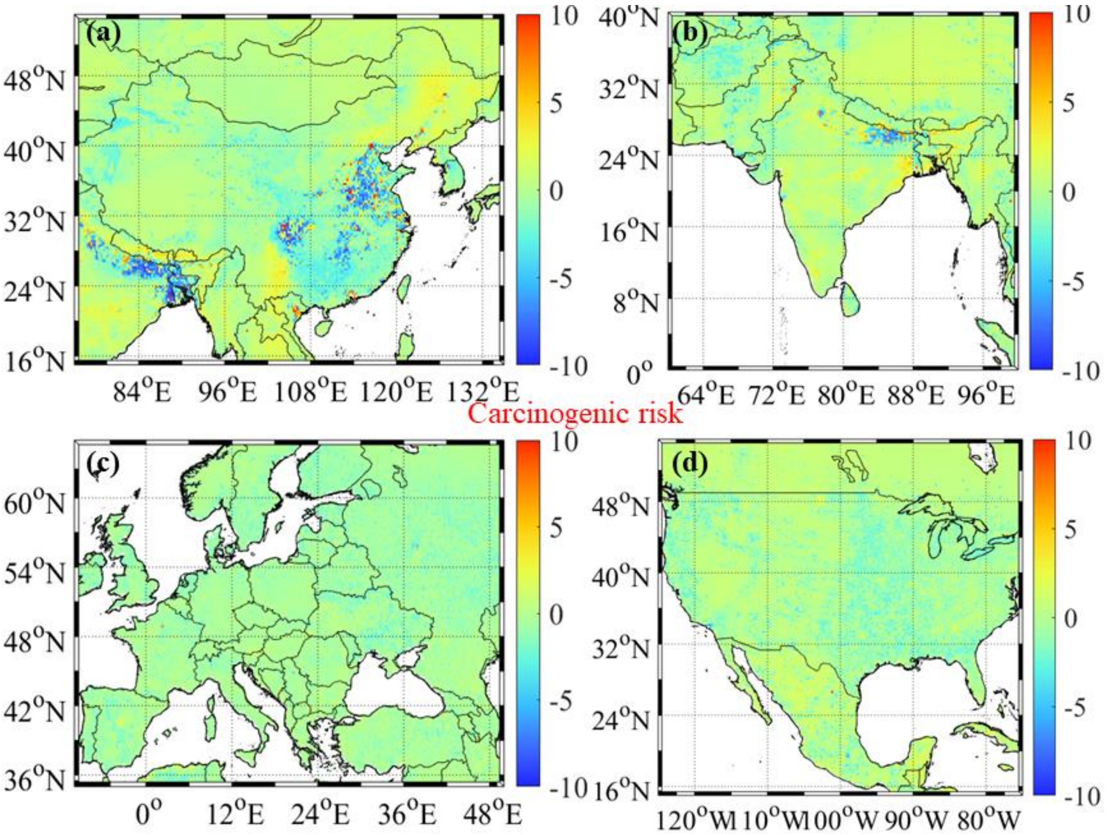

Figure 6 The non-carcinogenic risk differences (Unit: 10^{-3}) for atmospheric benzene between COVID-19 period in 2020 and the same period in 2019 in East Asia, South Asia, Europe, and North America (Difference = benzene concentration in 2020-benzene concentration in 2019).

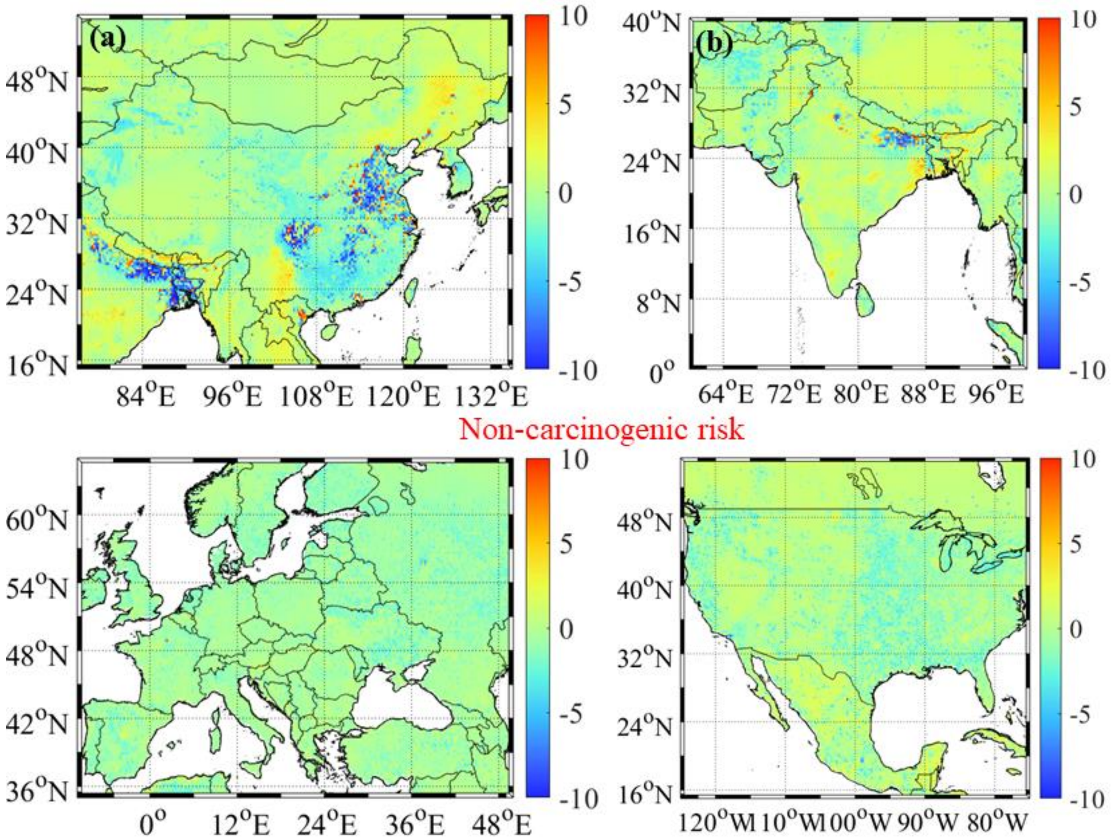

Table 1 The change ratio (%) of deweathered (P_{dew}) and detrended (P^*) benzene concentrations in major regions around the world.

Change ratio	China	India	Europe	United States
P_{dew} in 2020	-15.6	-23.6	-21.9	-16.2
P_{dew} in 2019	-2.31	-7.40	-8.04	-10.2
P^*	-13.3	-16.2	-13.9	-6.00